Citation: Cell Death and Disease (2011) 2, e240; doi:10.1038/cddis.2011.117

www.nature.com/cddis

A new vicious cycle involving glutamate excitotoxicity, oxidative stress and mitochondrial dynamics

D Nguyen[1], MV Alavi[2], K-Y Kim[3], T Kang[1], RT Scott[3], YH Noh[1], JD Lindsey[1], B Wissinger[4], MH Ellisman[3], RN Weinreb[1], GA Perkins[3] and W-K Ju*,[1]

Glutamate excitotoxicity leads to fragmented mitochondria in neurodegenerative diseases, mediated by nitric oxide and *S*-nitrosylation of dynamin-related protein 1, a mitochondrial outer membrane fission protein. *Optic atrophy gene 1* (*OPA1*) is an inner membrane protein important for mitochondrial fusion. Autosomal dominant optic atrophy (ADOA), caused by mutations in OPA1, is a neurodegenerative disease affecting mainly retinal ganglion cells (RGCs). Here, we showed that OPA1 deficiency in an ADOA model influences *N*-methyl-D-aspartate (NMDA) receptor expression, which is involved in glutamate excitotoxicity and oxidative stress. *Opa1*$^{enu/+}$ mice show a slow progressive loss of RGCs, activation of astroglia and microglia, and pronounced mitochondrial fission in optic nerve heads as found by electron tomography. Expression of NMDA receptors (NR1, 2A, and 2B) in the retina of *Opa1*$^{enu/+}$ mice was significantly increased as determined by western blot and immunohistochemistry. Superoxide dismutase 2 (SOD2) expression was significantly decreased, the apoptotic pathway was activated as Bax was increased, and phosphorylated Bad and BcL-xL were decreased. Our results conclusively demonstrate that not only glutamate excitotoxicity and/or oxidative stress alters mitochondrial fission/fusion, but that an imbalance in mitochondrial fission/fusion in turn leads to NMDA receptor upregulation and oxidative stress. Therefore, we propose a new vicious cycle involved in neurodegeneration that includes glutamate excitotoxicity, oxidative stress, and mitochondrial dynamics.

Cell Death and Disease (2011) **2,** e240; doi:10.1038/cddis.2011.117; published online 8 December 2011
Subject Category: Neuroscience

Mutations in optic atrophy type 1 (OPA1), a dynamin-related GTPase involved in various processes related to mitochondrial inner membrane structural dynamics, are linked with autosomal dominant optic atrophy (ADOA), one of the most common forms of hereditary optic neuropathy.[1,2] ADOA is characterized by a moderate to severe decrease in visual acuity, color vision disturbance, central visual field defects, and temporal optic nerve pallor with juvenile onset.[3,4] The fundamental pathological characteristics based on post mortem examinations of donor eyes from deceased patients with ADOA are loss of retinal ganglion cells (RGCs) and thinning of the nerve fiber layer.[3,4] Emerging evidence suggests that mice carrying heterozygous mutations in the murine *OPA1* gene resemble the human disease phenotype and thus can be regarded as true models for ADOA.[5–7] Studies on these models provided further evidence for a causative connection between OPA1 mutations and ascending RGC death, making ADOA a true neurodegenerative disease.[8] Nevertheless, the functional role of OPA1 as well as the signaling mechanism between OPA1 mutations and RGC death in ADOA remains unknown. OPA1 has been linked to different, and in parts disputed, cellular functions, such as mtDNA stability, maintenance of mitochondrial electron transport, scavenger of reactive oxygen species, mitochondrial coupling, apoptotic signaling, and mitochondrial cristae remodeling.[9,10] There is only unanimous agreement that OPA1 is necessary for mitochondrial fusion, because from yeast, to worm, to fly, to man, all studies describe fragmented mitochondrial networks upon loss of OPA1 function.[11]

Recently, OPA1 has gained more attention from other field of studies, as scientists recognized the importance of mitochondrial dynamics in many neurodegenerative diseases, among them the most frequent and most prominent ones are Alzheimer's disease, Parkinson's disease, Huntington's disease, and amyotrophic lateral sclerosis.[12–14] Remarkably, glutamate excitotoxicity has been linked to mitochondrial dysfunction in both acute and chronic neurodegenerative disorders.[15–19] In addition, growing evidence suggests that glutamate excitotoxicity-induced oxidative stress mediates this mitochondrial dysfunction by disturbing the closely regulated balance between mitochondrial fission and fusion.[20–23] The pro-fission mitochondrial outer membrane protein dynamin-related protein 1 (DRP1) is *S*-nitrosylated upon high nitric oxide levels produced in

[1]The Sophie and Arthur Brody Laboratory for Optic Nerve Biology, Hamilton Glaucoma Center, Department of Ophthalmology, University of California San Diego, La Jolla, CA, USA; [2]Department of Biologie, Institut für Zoologie, Johannes-Gutenberg Universität Mainz, Mainz, Germany; [3]Center for Research on Biological Systems, National Center for Microscopy and Imaging Research, Department of Neuroscience, University of California San Diego School of Medicine, La Jolla, CA, USA and [4]Molecular Genetics Laboratory, Center for Ophthalmology, University Clinics Tuebingen, Tuebingen, Germany
*Corresponding author: W-K Ju, The Sophie and Arthur Brody Laboratory for Optic Nerve Biology, Hamilton Glaucoma Center, Department of Ophthalmology, University of California San Diego, 9415 Campus Point Drive, La Jolla, CA 92037-0946, USA. Tel: 858 246 0452; Fax: 858 822 4717; E-mail: danielju@glaucoma.ucsd.edu
Keywords: OPA1 mutation; NMDA receptors; oxidative stress; mitochondrial fragmentation; retinal ganglion cells; glutamate excitotoxicity
Abbreviations: ADOA, autosomal dominant optic atrophy; DRP1, dynamin-related protein 1; GCL, ganglion cell layer; GFAP, glial fibrillary acidic protein; IPL, inner plexiform layer; NMDA, N-methyl-d-aspartate; NR, NMDA receptor; ONH, optic nerve head; OPL, outer plexiform layer; *OPA1*, *optic atrophy gene 1*; pBad, phosphorylated Bad; RGCs, retinal ganglion cells; SOD2, superoxide dismutase 2
Received 02.5.11; revised 29.8.11; accepted 21.9.11; Edited by A Verkhratsky

response to β-amyloid protein.[22] In support of this, we showed previously that memantine, an uncompetitive *N*-methyl-D-aspartate (NMDA) glutamate receptor antagonist, is able to counteract RGC death in glaucomatous or ischemic retinas, by preventing OPA1-mediated release of cytochrome *c* from the mitochondria.[16,19] Further, increased OPA1 expression protects RGCs in a mouse model of glaucoma as well as restores mitochondrial morphology and promotes neuronal survival following excitotoxicity.[24,25] All of these findings place the loss of OPA1 downstream of glutamate excitotoxicity. Reactive oxygen species including superoxide radicals (O_2^-) induce oxidative stress in many neurodegenerative diseases including optic neuropathies.[26,27] Superoxide dismutases (SODs), cytosolic SOD1, and mitochondrial SOD2 are expressed in the ganglion cell layer (GCL) and inner plexiform layer (IPL) in the rodent retina.[28] Emerging evidence suggests that SOD2 has a protective role against neuronal cell death that induced by glutamate excitotoxicity and oxidative stress.[21] However, the relationship–between OPA1 mutation and SOD2 in the retina remain unknown.

Here we report that mutations in OPA1 in turn lead to the upregulation of NMDA glutamate receptors as well as the downregulation of mitochondrial SOD2 in the retina of heterozygous *Opa1*$^{enu/+}$ mice. These findings indicate that not only glutamate excitotoxicity influences the mitochondrial fission/fusion balance (as suggested before), but also that altered mitochondrial fusion affects glutamate excitotoxicity. Therefore, we suggest a new vicious cycle involved in neurodegeneration that includes glutamate excitotoxicity, oxidative stress, and mitochondrial dynamics.

Results

Mutant OPA1 induces RGC loss and fragmented mitochondria in RGC axons. The *Opa1*$^{enu/+}$ mouse strain carries heterozygously a single-point mutation (c.1065 + 5G→A) in intron 10 of the *OPA1* gene that results in an in-frame deletion of 27 amino-acid residues in the GTPase domain of the OPA1 protein.[5] Homozygous *Opa1*$^{enu/enu}$ mice are not viable and die during embryogenesis after E8.5.[5] Heterozygous *Opa1*$^{enu/+}$ mice show reduced OPA1 protein levels in all examined tissues as well as in the retina (Figures 1a–c).[5] To verify that RGCs indeed express OPA1, we retrogradely labeled RGCs using FluoroGold and found that OPA1 protein was present in RGCs in wild-type control mice (Figures 1d–f). The *Opa1*$^{enu/+}$ mice suffer from a slow and progressive RGC loss (Supplementary Figure 1 and Supplementary Table 1),[5,8] which was confirmed by TUNEL-positive RGCs (Figures 1g and h). RGC loss is accompanied by activation of both astroglia and microglia as indicated by significantly increased glial fibrillary acidic protein (GFAP) expression in the retinas of *Opa1*$^{enu/+}$ mice (Figure 2).

3D tomographic reconstructions showed detailed mitochondrial membrane structure including the packing arrangement, shape, and density of cristae (Figure 3). Most of the cristae in wild-type control mice have both tubular and lamellar compartments. However, some cristae are completely lamellar or completely tubular. In the example shown, both lamellar and tubular cristae extended transversely (Figures 3a–c). Mitochondria from *Opa1*$^{enu/+}$ mice appeared shorter and fragmented (Figures 3d–f). In contrast to the wild-type mitochondria, a few lamellar cristae are also arranged longitudinally (Figures 3e and f). There was no difference in mitochondrial volume density, defined as the volume occupied by mitochondria divided by the volume occupied by the axoplasm in terms of a percentage, in the optic nerve head (ONH) axons (Figure 3g). However, mitochondrial lengths were significantly decreased in the ONH axons of *Opa1*$^{enu/+}$ mice compared with wild-type controls (Figure 3h). In contrast, the number of mitochondria, normalized to the total area occupied by axons in each image, was significantly increased in the ONH axons of *Opa1*$^{enu/+}$ mice compared with wild-type controls (Figure 3i). Taken together, these results conclusively show that mutations in the murine *OPA1* gene results in increased mitochondrial fission in ONH axons of *Opa1*$^{enu/+}$ mice likely contributing to RGC loss. Please see the Supplementary Movies 1 and 2 for presentations of the 3D tomographic data.

Mutant OPA1 triggers the upregulation of NMDA receptors. Previous studies reported that increased OPA1 expression restores mitochondrial morphology and promotes neuronal survival following excitotoxicity, as well as protects RGCs in a mouse model of glaucoma.[24,25] On the other hand, it has been shown that glutamate excitotoxicity can alter mitochondrial dynamics in a process mediated by oxidative stress.[22] To determine whether impaired mitochondrial dynamics in the retina of *Opa1*$^{enu/+}$ mice has any influence on NMDA receptors, relative changes of NMDA receptor expression including *NR1*, *NR2A*, and *NR2B* were measured by western blot and immunohistochemistry analyses.

NR1, NR2A, and NR2B protein expressions were significantly increased by 1.75 ± 0.11-, 2.22 ± 0.18-, and 1.48 ± 0.28-fold, respectively, in quantitative western blot analyses of retinal extracts derived from *Opa1*$^{enu/+}$ mice compared with wild-type control mice (Figure 4a). These findings could be independently confirmed by immunohistochemical analyses. When the primary antibodies were omitted, as a control for NR1 and NR2A immunohistochemistry, there was no labeling by the secondary antibodies in the retinas of wild-type control mice (Figures 4b and e). NR1 immunoreactivity was present in the GCL of wild-type control mice (Figure 4c). In *Opa1*$^{enu/+}$ mice, NR1 could be detected in the GCL as well as in the IPL. NR1 immunoreactivity was increased in these two cell layers compared with wild-type control animals (Figure 4d). Similarly, NR2A immunoreactivity was present in the GCL of wild-type control mice (Figure 4f) and increased in the inner nuclear layer and GCL of *Opa1*$^{enu/+}$ mice (Figure 4g). However, for NR2B, antibody showed no difference. These results demonstrate for the first time that OPA1 mutation triggers the upregulation of NMDA receptors expression.

Mutant OPA1 decreases antioxidant enzyme *SOD2* gene and protein expressions. As neurodegenerative diseases have previously been associated with increased oxidative stress,[18] we examined the expression of antioxidant enzymes in *Opa1*$^{enu/+}$ mice. In comparison with wild-type control mice, quantitative PCR analyses showed that

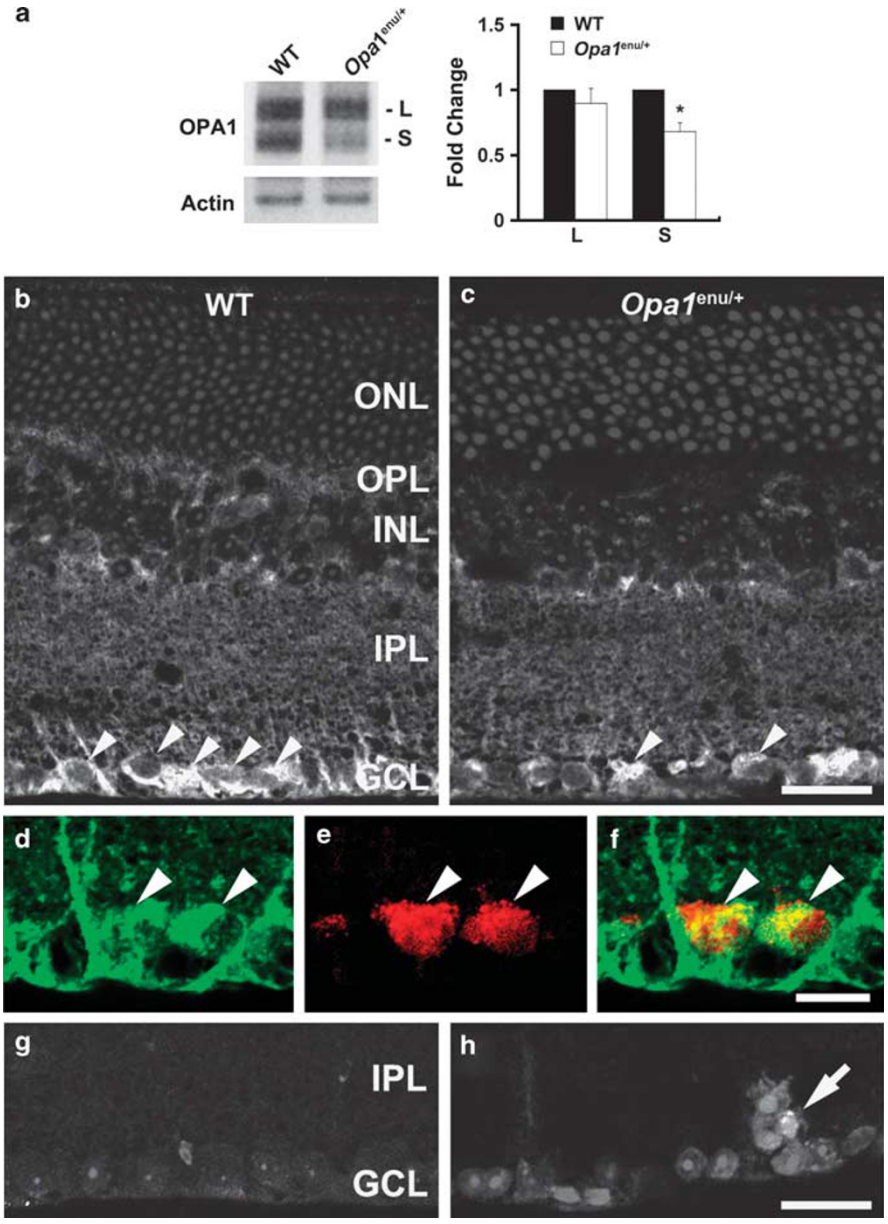

Figure 1 OPA1 mutation reduces OPA1 protein expression and induces apoptotic cell death in the retina of *Opa1*$^{enu/+}$ mice. (**a**) The OPA1 antibody recognized 90-kDa (L) and 80-kDa (S) isoforms of OPA1 protein in the total retinal protein extracts of wild-type control and *Opa1*$^{enu/+}$ mice. *Opa1*$^{enu/+}$ mice significantly decreased 80-kDa (S) isoform of OPA1 protein compared with wild-type control mice. Values are mean ± S.D. ($n = 4$ retinas/group). *Significant at $P < 0.05$ compared with wild-type control mice. (**b** and **c**) OPA1 immunohistochemistry. (**b**) OPA1 immunoreactivity was present in the GCL of wild-type control mouse (arrowheads). In contrast, OPA1 immunoreactivity was decreased in the GCL of *Opa1*$^{enu/+}$ mouse (arrowheads, **c**). (**d**–**f**) OPA1 (**d**) and FluoroGold (**e**) double labeling. Neurons containing OPA1 immunoractivity were colabeled by FluoroGold (arrowheads), indicating that RGCs contained OPA1 protein. There were no TUNEL-positive cells in the retina of wild-type control mouse (**g**) while apoptotic cell death was detectable in the GCL of the retina of *Opa1*$^{enu/+}$ mouse (arrow, **h**). ONL, outer nuclear layer; OPL, outer plexiform layer; INL, inner nuclear layer; GCL, ganglion cell layer. Scale bars, 20 μm (**b**–**e**)

SOD2 mRNA expression was significantly decreased by 0.68 ± 0.07-fold in the retinas of *Opa1*$^{enu/+}$ mice (Figure 5a). To confirm the downregulation of SOD2 protein levels, SOD2 protein expression was determined in the retinas of *Opa1*$^{enu/+}$ mice using western blot and immunohistochemistry analyses. As shown in Figure 5, quantitative western blot analyses of retinal extracts revealed that SOD2 protein expression was significantly decreased by 1.75 ± 0.11-fold in the retinas of *Opa1*$^{enu/+}$ mice compared with wild-type control mice (Figure 5b). This is also in agreement with the immunohistochemical analysis. When the primary antibody was omitted, as a control for SOD2 immunohistochemistry, there was no labeling by the secondary antibody in the retinas of wild-type control mice (Figure 5c). SOD2 immunoreactivity was present in the outer plexiform layer (OPL), IPL, and GCL of wild-type control mice (Figure 5d). However, SOD2 immunoreactivity was decreased in the OPL, IPL and GCL of *Opa1*$^{enu/+}$ mice (Figure 5e). These findings show that mitochondrial depletion of OPA1 associated with neurodegeneration of the optic

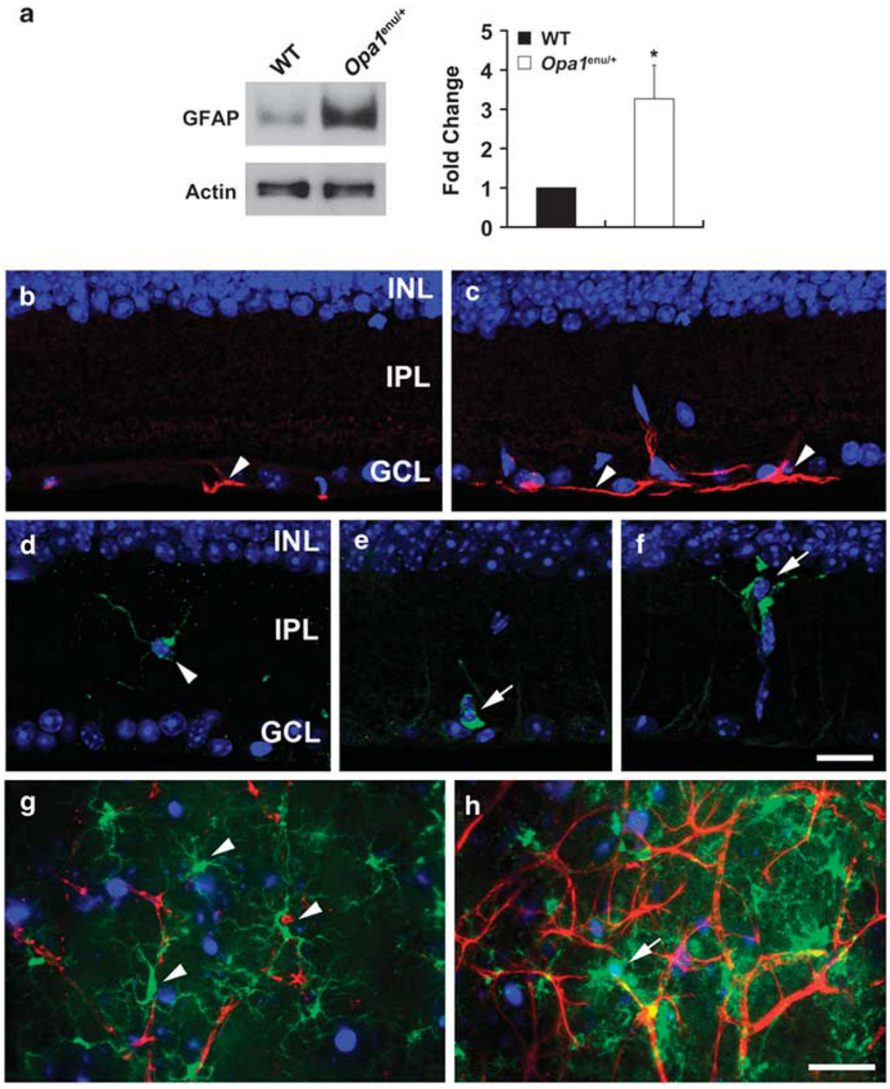

Figure 2 OPA1 mutation activates both astroglial and microglial cells in *Opa1*$^{enu/+}$ mice. (**a**) *Opa1*$^{enu/+}$ mice significantly increased GFAP expression compared with wild-type control mice. Values are mean ± S.D. ($n = 4$ retinas/group). *Significant at $P < 0.05$ compared with wild-type control mice. (**b** and **c**) GFAP immunohistochemistry. Compared with wild-type control mouse (**b**), *Opa1*$^{enu/+}$ mouse showed increased GFAP immunoreactivity in the GCL (arrowheads, **c**). (**d**–**f**) Iba1 immunohistochemistry. (**d**) Wild-type control mouse showed Iba1-positive ramified, quiescent microglial cell in the IPL (arrowhead). In contrast, *Opa1*$^{enu/+}$ mice showed Iba1-positive microglial cells that have shortened and thickened processes in the IPL (arrow, **e**) and GCL (arrow, **f**). (**g** and **h**) GFAP (red), Iba1 (green), and Fluorogold (blue) triple labeling. Note that FluoroGold-labeled RGC was engulfed by activated microglia cell in the GCL of *Opa1*$^{enu/+}$ mouse (arrow, **h**). INL, inner nuclear layer; GCL, ganglion cell layer. Scale bars, 20 μm (**b**–**h**)

nerve involves also oxidative stress in the mouse model for ADOA.

Mutant OPA1 activates the apoptotic pathway. As *Opa1*$^{enu/+}$ mice showed an increased number of TUNEL-positive apoptotic cells in the GCL when compared with wild-type control mice (Figures 1d and e), known key factors of the apoptotic cascade were examined for their expression and/or activity in the retina of *Opa1*$^{enu/+}$ mice and wild-type control mice. Quantitative PCR analyses demonstrated significantly increased *Bax* mRNA expression in *Opa1*$^{enu/+}$ mice compared with wild-type control mice by 1.32 ± 0.12-fold (Figure 6a). Consistent with this result, quantitative western blot analysis revealed that *Opa1*$^{enu/+}$ mice significantly increased Bax protein expression by 1.62 ± 0.27-fold in retinal extracts compared with wild-type control mice (Figure 6b). As the pro-apoptotic Bax/Bak is counteracted by the anti-apoptotic Bcl-xL, expression levels of Bcl-xL protein were assessed by western blot analysis. Intriguingly, *Opa1*$^{enu/+}$ mice significantly decreased Bcl-xL protein expression by 0.46 ± 0.2-fold in the retinal extracts compared with wild-type control mice (Figure 6b). Further, *Opa1*$^{enu/+}$ mice significantly decreased phosphorylated Bad (pBad) protein expression by 0.43 ± 0.08-fold in the retinal extracts compared with wild-type control mice (Figure 6b). When the primary antibody was omitted, as a control for Bcl-xL immunohistochemistry, there was no labeling by the secondary antibody in the retinas of wild-type control mice (Figure 6c). Bcl-xL immunoreactivity was present in the IPL and GCL of wild-type control mice (Figure 6d). However,

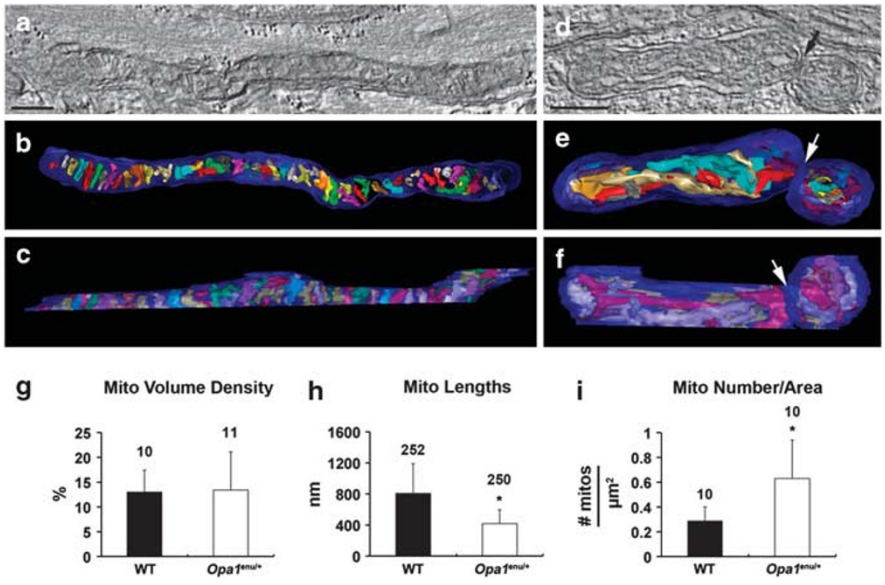

Figure 3 OPA1 mutation induces mitochondrial fission in the RGC axons in *Opa1*$^{enu/+}$ mice. OPA1-mutant mitochondria in optic nerve head axons display fissioning. (**a**–**c**) Tomographic reconstruction of a long mitochondrion from an adult wild-type control mouse. (**a**) A 2.4-nm slice through the center of a tomographic volume of an axon shows the mitochondrial membrane profiles and associations including those of outer and inner boundary membranes and cristae in a long mitochondrion with many cristae. Scale bar, 200 nm. (**b**) Top view and (**c**) side view of the segmented and surface-rendered volume showing the outer membrane (blue) and the entire complement of 51 cristae (various colors) provide a 3D snapshot of the packing arrangement, shape, and density of cristae. Most of the cristae have both tubular and lamellar compartments. However, some cristae are completely lamellar or completely tubular. Both lamellar and tubular cristae extend transversely. (**d**–**f**) Tomographic reconstruction of a shorter mitochondrion fragmented in two in an optic neve head axon from an adult OPA1-mutant mouse. (**d**) A 2.4-nm slice through the center of a tomographic volume of an axon shows the arrangement of outer and inner boundary membranes and cristae. The point of fission is indicated by the arrow. Note that the two fragmented portions are unequal in size. Scale bar, 200 nm. (**e**) Top view and (**f**) side view of the segmented and surface-rendered volume showing the outer membrane (blue) and the nine cristae in the left-hand fragment and the eight cristae in the right-hand fragment. The left-hand fragment has considerably more lamellar or mixed lamellar/tubular cristae than does the right-hand fragment. In contrast to the wild-type control mouse mitochondria, a few lamellar cristae are arranged longitudinally in the left fragment. Even though the outer membranes of the two fragments are touching, there is a clean break (arrows) between fragments. (**g**) There is no difference in mitochondrial volume density, defined as the volume occupied by mitochondria divided by the volume occupied by the axoplasm in terms of a percentage, in the optic nerve head axons. The bar is the mean and the error bar is the standard error of the mean. The number of measurements, corresponding to the number of images measured, is posted at the top of each bar. (**h**) Mitochondrial lengths are much shorter in *Opa1*$^{enu/+}$ mouse axons than in the wild-type control mouse axons by a factor of nearly two ($^*P<0.01$). The same images were used as in (**g**). (**i**) The number of mitochondria, normalized to the total area occupied by axons in each image, is much greater in *Opa1*$^{enu/+}$ mouse axons than in the wild-type control mouse axons by a factor greater than two ($^*P<0.01$)

Bcl-xL immunoreactivity was decreased in the IPL and GCL of *Opa1*$^{enu/+}$ mice (Figure 6e). This shows that the apoptotic pathway is activated in the retina of *Opa1*$^{enu/+}$ mice.

Discussion

ADOA is a true neurodegenerative disease affecting primarily RGCs.[3,4,8] Mutations in OPA1 account for at least 45% of all ADOA cases,[29] and the prevalence that a mutation carrier develops symptoms in his lifetime has been estimated to be 88%.[30] OPA1 is expressed ubiquitously,[1] and previous studies indicated that RGCs express OPA1 protein in rodent animals.[16,31] OPA1 mutations or deficiency impair mitochondrial fusion that results in fragmented mitochondria and apoptotic cell death in many cell types. More recently, it has been reported that OPA1 is involved in mitochondrial calcium homeostasis and mitochondrial dysfunction, suggesting a possible pathophysiological mechanism in RGC degeneration.[25,32,33] Accordingly, recent studies suggest that multisystemic neurological features can be found frequently in patients with OPA1 mutations.[34] The *Opa1*$^{enu/+}$ mouse is a true model for ADOA[5,8] and intriguingly, it also displays subclinical neurological and metabolic impairments.[7]

Consistent with these results, we found that *Opa1*$^{enu/+}$ mice had a greater RGC loss than wild-type control mice. Further, loss of RGCs in *Opa1*$^{enu/+}$ mice is not uniform, which is in agreement with the human pathology of ADOA. So far, there is no conclusive explanation for these regional differences and future studies need to address this in more detail. In addition, we found that astroglial and microglial cells were remarkably activated in the GCL of *Opa1*$^{enu/+}$ mice. Although it is possible that *Opa1* mutation-mediated retinal damage may be restricted in the GCL of *Opa1*$^{enu/+}$ mice, the signaling mechanism between OPA1 mutation and RGC death in the pathogenesis of ADOA remains unknown.

Glutamate excitotoxicity has been linked to OPA1-related mitochondrial dysfunction in retinal neurodegeneration including glaucoma.[16,19] Previously, we demonstrated that glutamate receptor activation triggers OPA1 release from the mitochondria in ischemic retinas, and that memantine, an uncompetitive NMDA glutamate receptor antagonist, blocks OPA1 and cytochrome *c* release, and apoptotic cell death in a mouse model of glaucoma.[16] Therefore, glutamate excitotoxicity may contribute to OPA1 alteration-mediated mitochondrial dysfunction and subsequent RGC death in retinal neurodegeneration. However, it is unknown how OPA1

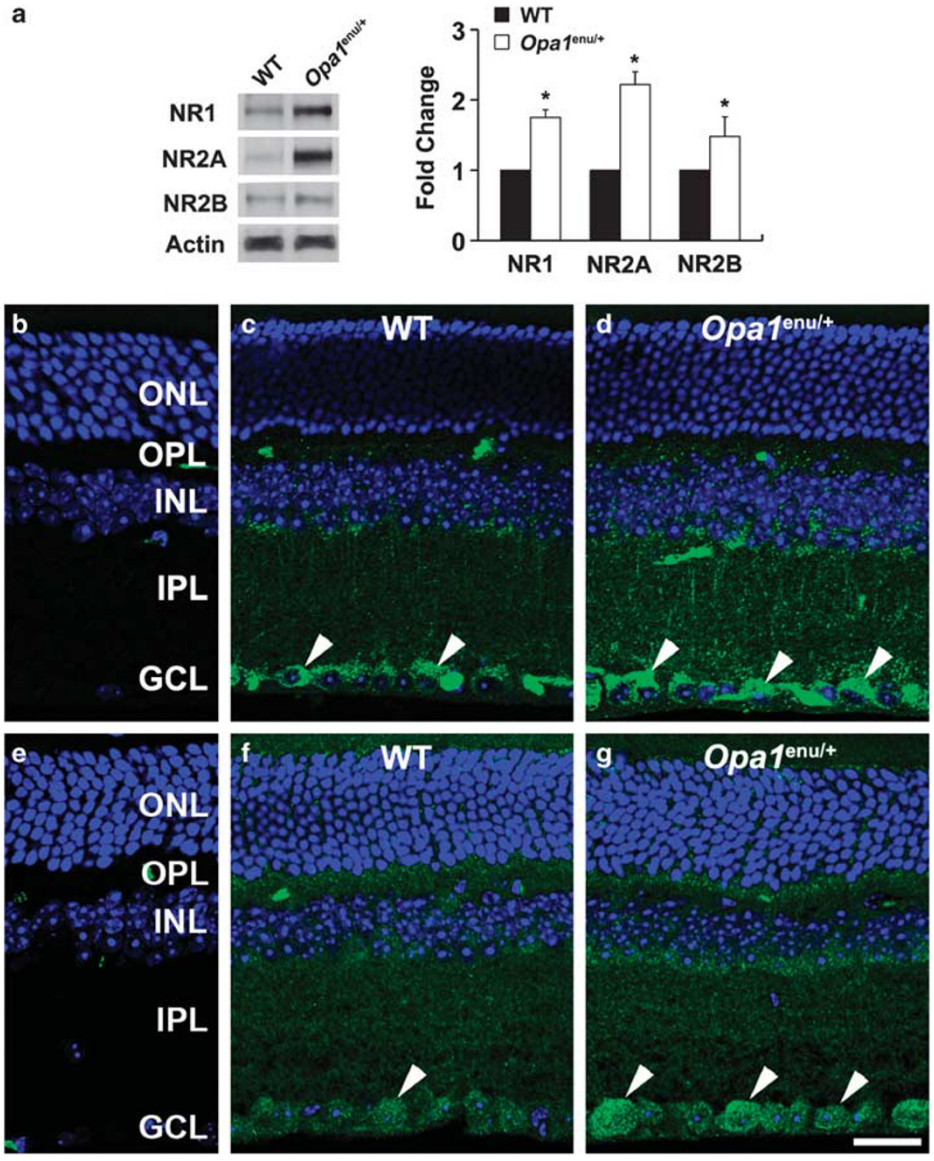

Figure 4 OPA1 mutation triggers activation of NMDA receptors in *Opa1*$^{enu/+}$ mice. (**a**) *Opa1*$^{enu/+}$ mice significantly increased NR1, NR2A, and NR2B protein expression compared with wild-type control mice. Values are mean ± S.D. ($n = 4$ retinas/group). *Significant at $P < 0.05$ compared with wild-type control mice. (**b**–**d**) NR1 immunohistochemistry. When the primary antibody for NR1 was omitted, there was no binding of the secondary antibody (**b**). Compared with wild-type control mouse (**c**), *Opa1*$^{enu/+}$ mouse showed increased NR1 immunoreactivity in the IPL and GCL (arrowheads, **d**). (**e**–**g**) NR2A immunohistochemistry. When the primary antibody for NR2A was omitted, there was no binding of the secondary antibody (**e**). Compared with wild-type control mouse (**f**), *Opa1*$^{enu/+}$ mouse showed increased NR2A immunoreactivity in the GCL (arrowheads, **g**). ONL, outer nuclear layer; OPL, outer nuclear layer; INL, inner nuclear layer; GCL, ganglion cell layer; NR, NMDA receptor. Scale bar, 20 μm (**b**–**g**)

mutation induces glutamate excitotoxicity and RGC death. In the present study, we found that NR1, NR2A, and NR2B protein expressions were significantly increased in the retinas of *Opa1*$^{enu/+}$ mice, and that immunoreactivities for NR1 and NR2A were increased mostly in the GCL of *Opa1*$^{enu/+}$ mice. Further, recent studies by our group as well as other investigators have shown that increased OPA1 expression protects RGCs in a mouse model of glaucoma as well as restores mitochondrial morphology and promotes neuronal survival following excitotoxicity.[24,25] Together with these findings, our results suggest that the mechanism by which RGC death is induced in *Opa1*$^{enu/+}$ mice involves OPA1 mutation-mediated glutamate excitotoxicity. Future studies will clarify whether this relationship has an important role in other neuropathies, since glutamate excitotoxicity has remarkably been linked to mitochondrial dysfunction in other neurodegenerative disorders.[15–18,35]

We observed that *SOD2* gene and protein expression were significantly decreased in the retinas of *Opa1*$^{enu/+}$ mice compared with wild-type control mice. It has been reported that overexpression of SOD2 in HT22 mouse hippocampal neuronal cells reduced the mitochondrial superoxide level, protected mitochondrial morphology and functions, and provided resistance against glutamate-induced oxidative

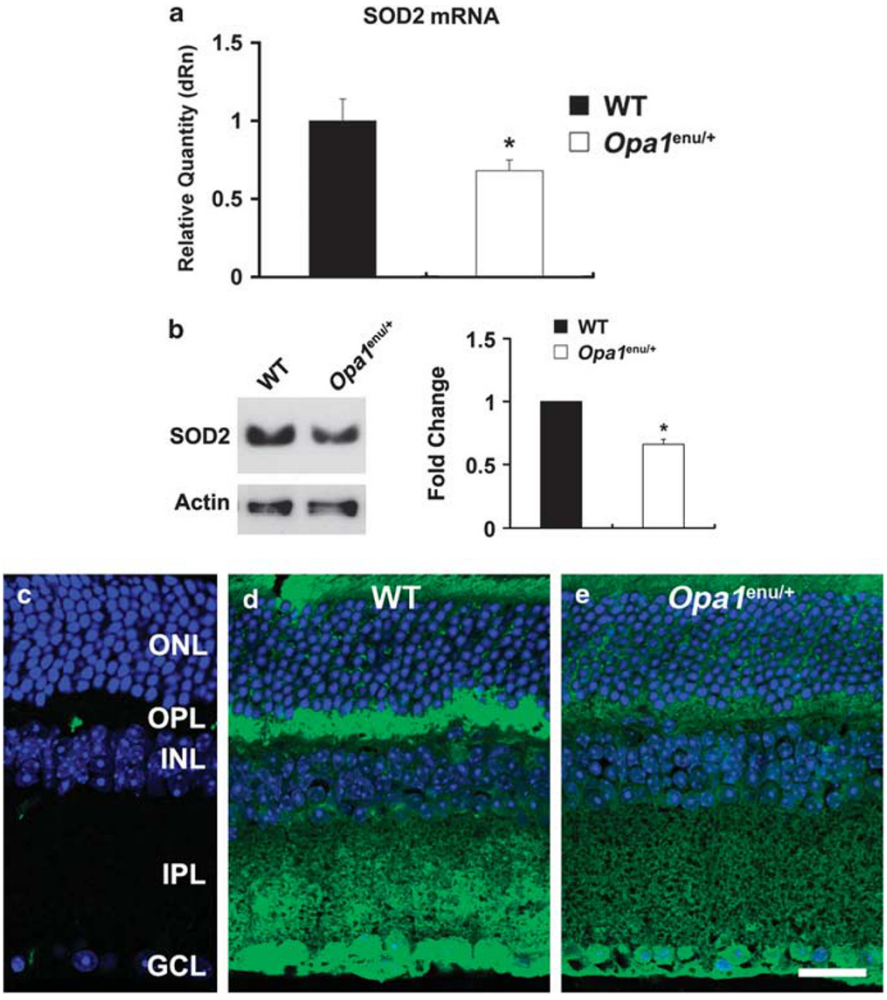

Figure 5 OPA1 mutation decreases *SOD2* gene and protein expression in *Opa1*$^{enu/+}$ mice. (**a**) *Opa1*$^{enu/+}$ mice significantly decreased SOD2 mRNA expression compared with wild-type control mice. (**b**) *Opa1*$^{enu/+}$ mice significantly decreased SOD2 protein expression compared with wild-type control mice. Values are mean ± S.D. ($n = 4$ retinas/group). *Significant at $P < 0.05$ compared with wild-type control mice. (**c**–**e**) SOD2 immunohistochemistry (green). When the primary antibody for SOD2 was omitted, there was no binding of the secondary antibody (**c**). Compared with wild-type control mouse (**d**), *Opa1*$^{enu/+}$ mouse showed decreased SOD2 immunoreactivity in the OPL, IPL and GCL (**e**). ONL, outer nuclear layer; OPL, outer nuclear layer; INL, inner nuclear layer; GCL, ganglion cell layer. Scale bar, 20 μm (**b**–**d**)

cytotoxicity, suggesting that SOD2 plays a critical role in protection against glutamate excitotoxicity-induced oxidative stress and cell death in neuronal cells.[21] Together with these findings, our observations raise the possibility that OPA1 mutation-mediated glutamate excitotoxicity may contribute to oxidative stress via a reduction of SOD2 expression in the retina of *Opa1*$^{enu/+}$ mice. Because a recent study suggested that upregulation of mitochondrial SOD2 by resveratrol represents an important mechanism for its protection against cytotoxicity resulting from mitochondrial oxidative stress, it is possible that the direct enhancement of *SOD2* gene expression in *Opa1*$^{enu/+}$ mice may provide new strategies to protect against RGC death. We believe that studying the benefits of blockade of glutamate excitotoxicity or inhibition of oxidative stress will be rewarding in many optic neuropathies including glaucoma, the most frequent blinding optic neuropathy in the Western countries.

In the present study, we found that mutant OPA1 significantly induces mitochondrial fission, altering mitochondrial dynamics. We also found an upregulation of NMDA receptors and a downregulation of SOD2. Modifications of this interconnection of glutamate excitotoxicity, oxidative stress, and mitochondrial morphology seem to be sufficient to induce the apoptotic pathway, because we found increased Bax expression as well as decreased Bcl-xL and phosphorylated Bad levels in the retina of *Opa1*$^{enu/+}$ mice. Bax is a pro-apoptotic member of the Bcl-2 family that is essential in many pathways of apoptosis,[36,37] as well as translocates to discrete foci on the mitochondria during the initial stages of apoptosis, which subsequently become mitochondrial scission sites.[38] It is counteracted by Bcl-xL, which was decreased in its expression in *Opa1*$^{enu/+}$ mice. Bcl-xL can form heterodimers with dephosphorylated Bad, which inactivates Bcl-xL and phosphorylation of Bad eliminates this dimerization, which activates Bcl-xL. This is in line with reduced levels of pBad and Bcl-xL, which may contribute to high Bax levels.

Previously, it has been shown that glutamate excitotoxicity leads to fragmented mitochondria in neurodegenerative diseases, mediated by nitric oxide and *S*-nitrosylation of

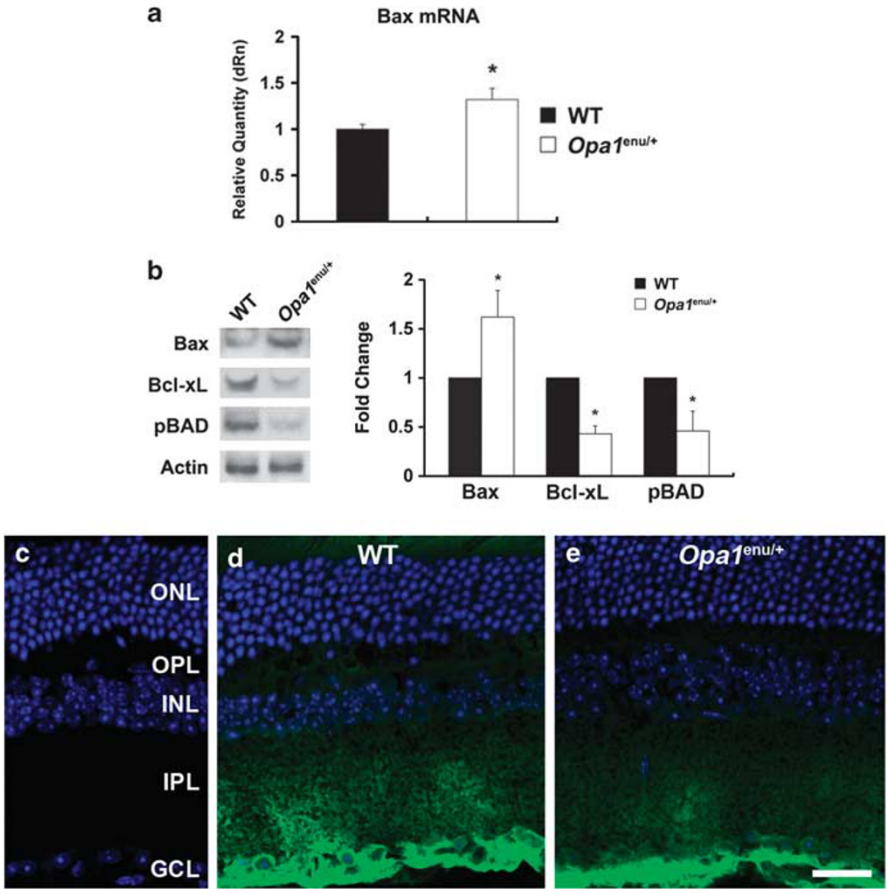

Figure 6 OPA1 mutation increases Bax expression, but decreases Bcl-xL and pBad expression in Opa1$^{enu/+}$ mice. (**a**) *Opa1*$^{enu/+}$ mice significantly increased Bax mRNA and protein expression compared with wild-type control mice. (**b**) *Opa1*$^{enu/+}$ mice significantly increased Bax protein expression, but decreased Bcl-xL and pBad protein expression compared with wild-type control mice. Values are mean ± S.D. ($n=4$ retinas/group). *Significant at $P<0.05$ compared with wild-type control mice. (**c**–**e**) Bcl-xL immunohistochemistry (green). When the primary antibody for Bcl-xL was omitted, there was no binding of the secondary antibody (**c**). Compared wild-type control mouse (**d**), *Opa1*$^{enu/+}$ mouse showed decreased Bcl-xL immunoreactivity in the IPL and GCL (**e**). ONL, outer nuclear layer; OPL, outer nuclear layer; INL, inner nuclear layer; GCL, ganglion cell layer. Scale bar, 20 μm (**c**–**e**)

DRP1, a mitochondrial pro-fission protein. Here we show that deficiency of a mitochondrial pro-fusion protein, OPA1, in turn upregulates NMDA receptors, which mediate glutamate excitotoxicity. This involves oxidative stress as a key factor and leads to the activation of the apoptotic pathway. Therefore, we suggest a new vicious cycle involved in neurodegeneration that includes glutamate excitotoxicity, oxidative stress, and mitochondrial dynamics. Intervention in this vicious cycle, by blockade of NMDA receptor activation, enhancement of SOD2 expression, or inhibition of the downstream apoptotic cascade may provide new strategies to protect neurons in neurodegenerative diseases, and in particular RGCs in optic neuropathies.

Materials and Methods

Animals and genotyping. The B6;C3-*Opa1*$^{329-355del}$ mouse line (herein referred to as *Opa1*$^{enu/+}$) as a model for ADOA has been described in details before.[5,7,8] All animals were housed in covered cages, fed with a standard rodent diet *ad libitum*, and kept on a 12-h light/12-h dark cycle. All procedures described were in accordance with the statement of the Association for Research in Vision and Ophthalmology for the use of animals in research.

Tissue preparation. Mice were anesthetized with isoflurane and/or intraperitoneal injection of a mixture of ketamine (100 mg/kg, Ketaset; Fort Dodge Animal Health, Fort Dodge, IA, USA) and xylazine (9 mg/kg, TranquiVed; VEDCO Inc., St. Joseph, MO, USA) before cervical dislocation. For immunohistochemistry, the retinas were dissected from the choroids and fixed with 4% paraformaldehyde in phosphate buffered saline (PBS, pH 7.4) for 2 h at 4°C. After several washes in PBS, the retinas were dehydrated through graded ethanols and embedded in polyester wax as described previously. For western blot analyses, whole retinas were immediately used or frozen in liquid nitrogen and stored at −70°C until use.

Immunohistochemical analysis. Immunohistochemical staining of 7-μm wax sections of full thickness retina or whole retina were performed as previously described.[31] Five sections per wax block from each group ($n=4$ retinas/group) were used for immunohistochemical analysis. Primary antibodies include mouse monoclonal anti-OPA1 antibody (1 : 1000; BD Transduction Laboratories, San Diego, CA, USA), mouse monoclonal anti-GFAP antibody (1 : 300; Sigma, St. Louis, MO, USA), rabbit polyclonal anti-Iba1 antibody (1 : 200; Wako Chemicals USA, Inc., Richmond, VA, USA), mouse monoclonal anti-NR1 antibody (1 : 1000; BD Pharmingen, San Diego, CA, USA), rabbit monoclonal anti-NR2A antibody (1 : 100; Millipore, Billerica, MA, USA), rabbit polyclonal anti-SOD2 antibody (1 : 5000; Santa Cruz Biotechnology, Inc., Santa Cruz, CA, USA), and rabbit polyclonal anti-Bcl-xL antibody (1 : 25; Cell Signaling, Danvers, MA, USA). To prevent non-specific background, tissues were incubated in 1% bovine serum albumin/PBS for 1 h at room temperature before incubation with the primary antibodies for 16 h at 4°C.

After several wash steps, the tissues were incubated with the secondary antibodies, Alexa Fluor 488 dye-conjugated goat anti-mouse IgG or Alexa Fluor 568 dye-conjugated goat anti-rabbit IgG (1 : 100; Invitrogen, Carlsbad, CA, USA) for 4 h at 4°C and subsequently washed with PBS. The sections were counterstained with the nucleic acid stain Hoechst 33342 (1 μg/ml, Invitrogen) in PBS. Images were acquired with confocal microscopy (Olympus FluoView1000; Olympus, Tokyo, Japan).

Western blot analysis. Retinas were dissected from the sclera of wild-type and *Opa1*$^{enu/+}$ mice. The retinal tissues were then immediately homogenized in a glass–teflon Potter homogenizer in lysis buffer (20 mM Hepes, pH 7.5/10 mM KCl/1.5 mM $MgCl_2$/1 mM EDTA/1 mM DTT/0.5% CHAPS/complete protease inhibitors; Roche Biochemicals, Indianapolis, IN, USA). Ten micrograms of pooled retinal protein ($n = 4$ retinas/group) from each group were separated by PAGE and electro-transferred to PVDF membranes. The membrane was blocked with 5% nonfat dry milk/0.5% Tween-20/PBS for 1 h and subsequently incubated with the primary antibodies overnight. The primary antibodies include mouse monoclonal anti-GFAP antibody (1 : 5000; Sigma), mouse monoclonal anti-NR1 antibody (1 : 1000; BD Pharmingen), rabbit monoclonal anti-NR2A antibody (1 : 500; Millipore), mouse monoclonal anti-NR2B antibody (1 : 1000; BD Biosciences, San Jose, CA, USA), rabbit polyclonal anti-SOD-2 antibody (1 : 5000; Santa Cruz Biotechnology), rabbit polyclonal anti-Bax antibody (1 : 500; Santa Cruz Biotechnology), rabbit polyclonal anti-Bcl-xL antibody (1 : 1000; Cell Signaling), mouse monoclonal anti-pBad antibody (1 : 2000; Cell Signaling), and mouse monoclonal anti-actin antibody (1 : 5000; Millipore). After several washes in Tween/PBS, the membranes were incubated with peroxidase-conjugated goat anti-mouse IgG (1 : 2000; Bio-Rad, Hercules, CA, USA) or goat anti-rabbit IgG (1 : 2000; Bio-Rad) and developed using chemiluminescence detection (ECL Plus, GE Healthcare Bio-Sciences, Piscataway, NJ, USA). Images were analyzed by digital fluorescence imager (Storm 860; GE Healthcare Bio-Sciences) and band densities were normalized using actin as total extracts calibrator with ImageQuant TL (GE Healthcare Bio-Sciences).

Quantitative PCR. Total RNA from retinal tissues ($n = 4$ retinas per group) was extracted with Trizol (Invitrogen), purified on RNeasy mini columns (Qiagen, Valencia, CA, USA), and treated with RNase-free DNAse I (Qiagen). The RNA purity was verified by confirming that the OD260 nm/280 nm absorption ratio exceeded 1.9. The cDNA was synthesized using SuperScript II first-strand RT-PCR kit (Invitrogen). *Bax*, *Bcl2*, and *SOD2* gene expression were measured by qPCR (MX3000P, Stratagene, La Jolla, CA, USA) using 25 ng of cDNA from retinas and 2 × universal PCR master mix (Applied Biosystems, Foster City, CA, USA) with a one-step program (95°C for 10 min, 95°C for 30 s, and 60°C for 1 min for 50 cycles). Primers for Bax, Bcl2, SOD2, and GAPDH, as well as Taqman probe for GAPDH were designed using Primer Express 2.0 software (Supplementary Table 2; Applied Biosystems), obtained from Biosearch Technologies (Novato, CA, USA). The probe for Bax, Bcl2, and SOD2 was obtained from the Roche Universal Probe Library (Roche Diagnostics, Mannheim, Germany), and the optimal concentrations for probe and primers were determined using heart tissue. Standard curves were constructed using nine twofold dilutions (50–0.195 ng) for both the targets and the endogenous reference (GAPDH). The samples were run in duplicate for each target and endogenous GAPDH control.

Electron microscopy. For conventional electron microscopy (EM), two eyes from each group ($n = 2$ mice) were fixed via cardiac perfusion with solution at 37°C in 2% paraformaldehyde, 2.5% glutaraldehyde (Ted Pella, Redding, CA, USA) in 0.15 M sodium cacodylate (pH 7.4) and placed in pre-cooled fixative on ice for 1 h. The following procedure was used to optimize mitochondrial structural preservation and membrane contrast.[39] The retinas were dissected with 0.15 M sodium cacodylate plus 3 mM calcium chloride (pH 7.4) on ice and then post-fixed with 1% osmium tetroxide, 0.8% potassium ferrocyanide, 3 mM calcium chloride in 0.1 M sodium cacodylate (pH 7.4) for 1 h, washed with ice-cold distilled water, poststained with 2% uranyl acetate at 4°C, dehydrated using graded ethanol, and embedded in Durcupan resin (Fluka, St. Louis, MO, USA). Ultrathin (70 nm) sections were poststained with uranyl acetate and lead salts, and evaluated by a JEOL 1200FX transmission EM operated at 80 kV. Images were recorded on film at × 8000 magnification. The negatives were digitized at 1800 d.p.i. using a Nikon Cool scan system, giving an image size of 4033 × 6010 pixel array and a pixel resolution of 1.77 nm.[39] For quantitative analysis, the number of mitochondria was normalized to the total area occupied by axons in each image, which was measured using ImageJ (NIH, Bethesda, MD, USA). Mitochondrial lengths were measured with ImageJ. The mitochondrial volume density, defined as the volume occupied by mitochondria divided by the volume occupied by the axoplasm, was estimated using stereology as follows. A 112 × 112 square grid (112 × 112 chosen for ease of use with Photoshop) was overlaid on each image loaded in Photoshop (Adobe), and mitochondria and axoplasm lying under intercepts were counted. The relative volume of mitochondria was expressed as the ratio of intercepts coinciding with this organelle relative to the intercepts coinciding with axoplasm.

Electron microscope tomography. Sections of retinas from each group were cut at thicknesses of 400–500 nm. Sections were then stained 30 min in 2% aqueous uranyl acetate, followed by 15 min in lead salts. Fiducial cues consisting of 20 nm and colloidal gold particles were deposited on opposite sides of the section. For each reconstruction, a series of images at regular tilt increments was collected with a JEOL 4000EX intermediate-voltage electron microscope operated at 400 kV. The specimens were irradiated before initiating a tilt series in order to limit anisotropic specimen thinning during image collection. Tilt series were recorded using a 4k × 4k CCD camera with an angular increment of 2° from −60° to +60° about an axis perpendicular to the optical axis of the microscope using a computer-controlled goniometer to increment accurately the angular steps. The illumination was held to near parallel beam conditions and optical density maintained constant by varying the exposure time. The magnification was × 12 000 and the pixel resolution was 01.2 nm. The IMOD package was used for rough alignment with the fine alignment and reconstruction performed using the TxBR package.[40] Volume segmentation was performed by manual tracing in the planes of highest resolution with the program Xvoxtrace.[40] The mitochondrial reconstructions were visualized using Analyze (Mayo Foundation, Rochester, MN, USA) or the surface-rendering graphics of Synu (National Center for Microscopy and Imaging Research, San Diego, CA, USA) as described by Perkins *et al*.[40] These programs allow one to step through slices of the reconstruction in any orientation and to track or model features of interest in three dimensions. Measurements of mitochondrial outer, inner boundary, and cristae membrane surface areas and volumes were made within segmented volumes by the programs Synuarea and Synuvolume, respectively (National Center for Microscopy and Imaging Research). These were used to determine the cristae density, defined as the ratio: sum of the cristae volumes divided by the mitochondrial volume. Movies of the tomographic volume were made using Amira.

Retrograde labeling of RGCs. One week before killing, FluoroGold (1 μl/injection of 4% solution; Fluorochrome Inc., Englewood, CO, USA) diluted in saline was injected bilaterally into the superior colliculi of anesthetized mice with a mixture of ketamine and xylazine in a stereotactic apparatus as previously described.[31] FluoroGold is taken up by the axon terminals of the RGCs and transported retrogradely to the somas in the retina. Images of the FluoroGold-labeled RGCs were captured under an Olympus spinning disk confocal microscope (Olympus America Inc., Center Valley, PA, USA) equipped with a high-precision closed loop XY stage and closed loop Z control with commercial mosaic acquisition software (MicroBrightField; MBF Bioscience Inc., Williston, VT, USA). The microscope is equipped with high-resolution high-sensitive CCD camera for high-speed mosaic acquisition. The numbers of RGCs in the central, middle, and peripheral retina were counted in a masked manner and averaged. Care was taken to count only RGCs and not microglia based on the difference between their morphologies.

TUNEL staining. Sections were incubated with proteinase K (10 μg/ml, 10 mM Tris, pH 7.4–8.0) for 10 min at 37°C. After rinsing in PBS, the sections were incubated with terminal deoxynucleotidyl transferase plus nucleotide mixture in reaction buffer for 60 min at 37°C (*In situ* Cell Death Detection kit, Roche Applied Science, Indianapolis, IN, USA) as previously described.

Statistical analysis. Data were presented as the mean ± S.D. Comparison of two experimental conditions was evaluated using the unpaired Student's *t*-test. $P < 0.05$ was considered to be statistically significant.

Conflict of Interest

The authors declare no conflict of interest.

Acknowledgements. This work was supported, in part, by NIH grants Summer Research Training (DN), NCRR P41 RR004050 (MHE), and EY018658 (WKJ). We thank Karen Duong-Polk for technical assistance for animal maintenance and genotyping.

1. Alexander C, Votruba M, Pesch UE, Thiselton DL, Mayer S, Moore A *et al.* OPA1, encoding a dynamin-related GTPase, is mutated in autosomal dominant optic atrophy linked to chromosome 3q28. *Nat Genet* 2000; **26**: 211–215.
2. Delettre C, Lenaers G, Griffoin JM, Gigarel N, Lorenzo C, Belenguer P *et al.* Nuclear gene OPA1, encoding a mitochondrial dynamin-related protein, is mutated in dominant optic atrophy. *Nat Genet* 2000; **26**: 207–210.
3. Johnston PB, Gaster RN, Smith VC, Tripathi RC. A clinicopathologic study of autosomal dominant optic atrophy. *Am J Ophthalmol* 1979; **88**: 868–875.
4. Kjer P, Jensen OA, Klinken L. Histopathology of eye, optic nerve and brain in a case of dominant optic atrophy. *Acta Ophthalmol (Copenh)* 1983; **61**: 300–312.
5. Alavi MV, Bette S, Schimpf S, Schuettauf F, Schraermeyer U, Wehrl HF *et al.* A splice site mutation in the murine Opa1 gene features pathology of autosomal dominant optic atrophy. *Brain* 2007; **130** (Part 4): 1029–1042.
6. Davies VJ, Hollins AJ, Piechota MJ, Yip W, Davies JR, White KE *et al.* Opa1 deficiency in a mouse model of autosomal dominant optic atrophy impairs mitochondrial morphology, optic nerve structure and visual function. *Hum Mol Genet* 2007; **16**: 1307–1318.
7. Alavi MV, Fuhrmann N, Nguyen HP, Yu-Wai-Man P, Heiduschka P, Chinnery PF *et al.* Subtle neurological and metabolic abnormalities in an Opa1 mouse model of autosomal dominant optic atrophy. *Exp Neurol* 2009; **220**: 404–409.
8. Heiduschka P, Schnichels S, Fuhrmann N, Hofmeister S, Schraermeyer U, Wissinger B *et al.* Electrophysiological and histologic assessment of retinal ganglion cell fate in a mouse model for OPA1-associated autosomal dominant optic atrophy. *Invest Ophthalmol Vis Sci* 2010; **51**: 1424–1431.
9. Yu-Wai-Man P, Sitarz KS, Samuels DC, Griffiths PG, Reeve AK, Bindoff LA *et al.* OPA1 mutations cause cytochrome *c* oxidase deficiency due to loss of wild-type mtDNA molecules. *Hum Mol Genet* 2010; **19**: 3043–3052.
10. Cipolat S, Rudka T, Hartmann D, Costa V, Serneels L, Craessaerts K *et al.* Mitochondrial rhomboid PARL regulates cytochrome *c* release during apoptosis via OPA1-dependent cristae remodeling. *Cell* 2006; **126**: 163–175.
11. Westermann B. Mitochondrial dynamics in model organisms: what yeasts, worms and flies have taught us about fusion and fission of mitochondria. *Semin Cell Dev Biol* 2010; **21**: 542–549.
12. Cho DH, Nakamura T, Lipton SA. Mitochondrial dynamics in cell death and neurodegeneration. *Cell Mol Life Sci* 2010; **67**: 3435–3447.
13. Su B, Wang X, Zheng L, Perry G, Smith MA, Zhu X. Abnormal mitochondrial dynamics and neurodegenerative diseases. *Biochim Biophys Acta* 2010; **1802**: 135–142.
14. Morais VA, De Strooper B. Mitochondria dysfunction and neurodegenerative disorders: cause or consequence. *J Alzheimers Dis* 2010; **20** (Suppl 2): S255–S263.
15. Nicholls DG, Ward MW. Mitochondrial membrane potential and neuronal glutamate excitotoxicity: mortality and millivolts. *Trends Neurosci* 2000; **23**: 166–174.
16. Ju WK, Kim KY, Angert M, Duong-Polk KX, Lindsey JD, Ellisman MH *et al.* Memantine blocks mitochondrial OPA1 and cytochrome *c* release and subsequent apoptotic cell death in glaucomatous retina. *Invest Ophthalmol Vis Sci* 2009; **50**: 707–716.
17. Fan MM, Raymond LA. *N*-methyl-D-aspartate (NMDA) receptor function and excitotoxicity in Huntington's disease. *Prog Neurobiol* 2007; **81**: 272–293.
18. Beal MF. Aging, energy, and oxidative stress in neurodegenerative diseases. *Ann Neurol* 1995; **38**: 357–366.
19. Ju WK, Lindsey JD, Angert M, Patel A, Weinreb RN. Glutamate receptor activation triggers OPA1 release and induces apoptotic cell death in ischemic rat retina. *Mol Vis* 2008; **14**: 2629–2638.
20. Fukui M, Choi HJ, Zhu BT. Mechanism for the protective effect of resveratrol against oxidative stress-induced neuronal death. *Free Radic Biol Med* 2010; **49**: 800–813.
21. Fukui M, Zhu BT. Mitochondrial superoxide dismutase SOD2, but not cytosolic SOD1, plays a critical role in protection against glutamate-induced oxidative stress and cell death in HT22 neuronal cells. *Free Radic Biol Med* 2010; **48**: 821–830.
22. Cho DH, Nakamura T, Fang J, Cieplak P, Godzik A, Gu Z *et al.* S-nitrosylation of Drp1 mediates beta-amyloid-related mitochondrial fission and neuronal injury. *Science* 2009; **324**: 102–105.
23. Nakamura T, Cieplak P, Cho DH, Godzik A, Lipton SA. S-nitrosylation of Drp1 links excessive mitochondrial fission to neuronal injury in neurodegeneration. *Mitochondrion* 2010; **10**: 573–578.
24. Ju WK, Kim KY, Duong-Polk KX, Lindsey JD, Ellisman MH, Weinreb RN. Increased optic atrophy type 1 expression protects retinal ganglion cells in a mouse model of glaucoma. *Mol Vis* 2010; **16**: 1331–1342.
25. Jahani-Asl A, Pilon-Larose K, Xu W, MacLaurin JG, Park DS, McBride HM *et al.* The mitochondrial inner membrane GTPase, optic atrophy 1 (Opa1), restores mitochondrial morphology and promotes neuronal survival following excitotoxicity. *J Biol Chem* 2011; **286**: 4772–4782.
26. Qi X, Lewin AS, Hauswirth WW, Guy J. Optic neuropathy induced by reductions in mitochondrial superoxide dismutase. *Invest Ophthalmol Vis Sci* 2003; **44**: 1088–1096.
27. Qi X, Hauswirth WW, Guy J. Dual gene therapy with extracellular superoxide dismutase and catalase attenuates experimental optic neuritis. *Mol Vis* 2007; **13**: 1–11.
28. Oguni M, Tanaka O, Tamura H, Shinohara H, Kato K, Setogawa T. Ontogeny of copper-zinc and manganese superoxide dismutase in the developing rat retina: immunohistochemical and immunochemical study. *Ophthalmic Res* 1995; **27**: 227–233.
29. Fuhrmann N, Alavi MV, Bitoun P, Woernle S, Auburger G, Leo-Kottler B *et al.* Genomic rearrangements in OPA1 are frequent in patients with autosomal dominant optic atrophy. *J Med Genet* 2009; **46**: 136–144.
30. Fuhrmann N, Schimpf S, Kamenisch Y, Leo-Kottler B, Alexander C, Auburger G *et al.* Solving a 50 year mystery of a missing OPA1 mutation: more insights from the first family diagnosed with autosomal dominant optic atrophy. *Mol Neurodegener* 2010; **5**: 25.
31. Ju WK, Misaka T, Kushnareva Y, Nakagomi S, Agarwal N, Kubo Y *et al.* OPA1 expression in the normal rat retina and optic nerve. *J Comp Neurol* 2005; **488**: 1–10.
32. Kamei S, Chen-Kuo-Chang M, Cazevieille C, Lenaers G, Olichon A, Belenguer P *et al.* Expression of the Opa1 mitochondrial protein in retinal ganglion cells: its downregulation causes aggregation of the mitochondrial network. *Invest Ophthalmol Vis Sci* 2005; **46**: 4288–4294.
33. Dayanithi G, Chen-Kuo-Chang M, Viero C, Hamel C, Muller A, Lenaers G. Characterization of Ca2+ signalling in postnatal mouse retinal ganglion cells: involvement of OPA1 in Ca2+ clearance. *Ophthalmic Genet* 2010; **31**: 53–65.
34. Yu-Wai-Man P, Griffiths PG, Gorman GS, Lourenco CM, Wright AF, Auer-Grumbach M *et al.* Multi-system neurological disease is common in patients with OPA1 mutations. *Brain* 2010; **133** (Part 3): 771–786.
35. Mattson MP, Pedersen WA, Duan W, Culmsee C, Camandola S. Cellular and molecular mechanisms underlying perturbed energy metabolism and neuronal degeneration in Alzheimer's and Parkinson's diseases. *Ann NY Acad Sci* 1999; **893**: 154–175.
36. Wasiak S, Zunino R, McBride HM. Bax/Bak promote sumoylation of DRP1 and its stable association with mitochondria during apoptotic cell death. *J Cell Biol* 2007; **177**: 439–450.
37. Wei MC, Zong WX, Cheng EH, Lindsten T, Panoutsakopoulou V, Ross AJ *et al.* Proapoptotic BAX and BAK: a requisite gateway to mitochondrial dysfunction and death. *Science* 2001; **292**: 727–730.
38. Arnoult D, Rismanchi N, Grodet A, Roberts RG, Seeburg DP, Estaquier J *et al.* Bax/Bak-dependent release of DDP/TIMM8a promotes Drp1-mediated mitochondrial fission and mitoptosis during programmed cell death. *Curr Biol* 2005; **15**: 2112–2118.
39. Barsoum MJ, Yuan H, Gerencser AA, Liot G, Kushnareva Y, Graber S *et al.* Nitric oxide-induced mitochondrial fission is regulated by dynamin-related GTPases in neurons. *EMBO J* 2006; **25**: 3900–3911.
40. Perkins GA, Renken CW, Song JY, Frey TG, Young SJ, Lamont S *et al.* Electron tomography of large, multicomponent biological structures. *J Struct Biol* 1997; **120**: 219–227.

Supplementary Information accompanies the paper on Cell Death and Disease website (http://www.nature.com/cddis)